OXFORD

Human Molecular Genetics, 2017, Vol. 26, No. 15 2897–2911

doi: 10.1093/hmg/ddx171
Advance Access Publication Date: 5 May 2017
Original Article

ORIGINAL ARTICLE

The chaperone activity of 4PBA ameliorates the skeletal phenotype of *Chihuahua*, a zebrafish model for dominant osteogenesis imperfecta

Roberta Gioia[1,†], Francesca Tonelli[1,†], Ilaria Ceppi[1], Marco Biggiogera[2], Sergey Leikin[3], Shannon Fisher[4], Elena Tenedini[5], Timur A. Yorgan[6], Thorsten Schinke[6], Kun Tian[7], Jean-Marc Schwartz[7], Fabiana Forte[8], Raimund Wagener[8], Simona Villani[9], Antonio Rossi[1] and Antonella Forlino[1,*]

[1]Department of Molecular Medicine, Biochemistry Unit, University of Pavia, Pavia, Italy, [2]Department of Biology and Biotechnology, University of Pavia, Pavia, Italy, [3]Section on Physical Biochemistry, Eunice Kennedy Shriver NICHD, NIH, Bethesda, MD, USA, [4]Department of Pharmacology & Experimental Therapeutics, Boston University School of Medicine, Boston, MA, USA, [5]Center for Genome Research, Department of Medical and Surgical Sciences, University of Modena and Reggio Emilia, Modena, Italy, [6]Institute of Osteology and Biomechanic, Center for Experimental Medicine, University of Hamburg, Hamburg, Germany, [7]Faculty of Biology, Medicine and Health, University of Manchester, Manchester, UK, [8]Medical Faculty, Center for Biochemistry, Center for Molecular Medicine, University of Cologne, Cologne, Germany and [9]Department of Public Health and Experimental and Forensic Medicine, Unit of Biostatistics and Clinical Epidemiology, University of Pavia, Pavia, Italy

*To whom correspondence should be addressed at: Department of Molecular Medicine, Biochemistry Unit, University of Pavia, Via Taramelli 3/B, 27100 Pavia, Italy. Tel: +39 0382 987235; Fax: +39-0382-423108; Email: aforlino@unipv.it

Abstract

Classical osteogenesis imperfecta (OI) is a bone disease caused by type I collagen mutations and characterized by bone fragility, frequent fractures in absence of trauma and growth deficiency. No definitive cure is available for OI and to develop novel drug therapies, taking advantage of a repositioning strategy, the small teleost zebrafish (*Danio rerio*) is a particularly appealing model. Its small size, high proliferative rate, embryo transparency and small amount of drug required make zebrafish the model of choice for drug screening studies, when a valid disease model is available. We performed a deep characterization of the zebrafish mutant *Chihuahua*, that carries a G574D (p.G736D) substitution in the α1 chain of type I collagen. We successfully validated it as a model for classical OI. Growth of mutants was delayed compared with WT. X-ray, μCT, alizarin red/alcian blue and calcein staining revealed severe skeletal deformity, presence of fractures and delayed mineralization. Type I collagen extracted from different tissues showed abnormal electrophoretic migration and low melting temperature. The presence of endoplasmic reticulum (ER) enlargement due to mutant collagen retention in osteoblasts and

[†]These authors contributed equally to this work.

Received: February 17, 2017. **Revised:** April 28, 2017. **Accepted:** May 2, 2017

fibroblasts of mutant fish was shown by electron and confocal microscopy. Two chemical chaperones, 4PBA and TUDCA, were used to ameliorate the cellular stress and indeed 4PBA ameliorated bone mineralization in larvae and skeletal deformities in adult, mainly acting on reducing ER cisternae size and favoring collagen secretion. In conclusion, our data demonstrated that ER stress is a novel target to ameliorate OI phenotype; chemical chaperones such as 4PBA may be, alone or in combination, a new class of molecules to be further investigated for OI treatment.

Introduction

Osteogenesis imperfecta (OI, OMIM # 166200, 166210, 259420, 166220) is a heritable skeletal disease mainly caused by dominant mutations in *COL1A1* or *COL1A2* genes coding for the α1 and α2 chain of type I collagen, the most abundant component of the bone organic matrix (1). Additional dominant and recessive OI forms due to mutations in other genes have been described, all affecting the synthesis, secretion, processing or matrix incorporation of type I collagen or the osteoblasts differentiation and activity, and all sharing the abnormal skeletal phenotype (2). Bone fragility, skeletal deformity and growth delay were traditionally exclusively attributed to the presence of an altered extracellular matrix. More recently, a role of abnormal osteoblasts homeostasis due to the mutant collagen retention and affecting cell differentiation and activity has been hypothesized as a relevant player in modulating OI pathophysiology, opening new opportunities for the treatment of the disease (3,4).

A different ability to cope with intracellular stress modulates the phenotypic outcome of the Brtl mouse, a well characterized model for classical OI (3,5). Brtl carries in heterozygosis a typical glycine substitution (G349C) in the α1(I) chain and, in presence of the same causative mutation, shows either a lethal or a moderately severe phenotype (6). In lethal mice an up-regulation of molecules involved in apoptosis and protein degradation was detected, whereas in mice with a moderately severe outcome the up-regulation of chaperones was described (3,5). More recently, we showed a different cytoskeletal assembly in lethal Brtl cells; our data demonstrated that compromised cytoskeletal organization impaired both cell signaling and cellular trafficking specifically in mutant lethal mice, altering bone properties (7). These results suggested that a disturbed intracellular homeostasis in bone cells could modulate OI outcome. Indeed, osteoblast malfunctioning was reported to negatively affect bone properties also in a different murine model for dominant OI, the Amish mouse (*Col1a2*$^{tm1Mcbr/J}$) carrying a G610C substitution in the α2(I) chain (8,9).

Based on these observations, the targeting of osteoblast malfunction, favoring either mutant collagen refolding and secretion or its selective intracellular degradation, seems particularly attractive to ameliorate OI outcome. No definitive therapy is so far available for OI and the correction of the genetic defect by gene/cell therapy approaches, although particularly appealing, will require long time and efforts. In the meantime, the search for novel drugs able to improve the quality of life represents a strong patients' demand. Furthermore, since cellular stress has been found not only in classical dominant OI, but also in several novel recessive OI forms due to mutations in protein affecting collagen post-translational modifications, it may represent a common and valuable target for multiple OI types. The availability of various molecules already approved by Food and Drug Administration (FDA) for other purposes and usable in a repositioning approach will facilitate the transition from the bench to the bedsite, allowing to skip pharmacokinetics tests and phase I safety trials (10).

Among the others, 4 phenylbutyrate (4PBA) and tauroursodeoxycholic acid (TUDCA) are two well-known molecules approved for urea cycle disorders and cholestasis respectively, and known to have other functions (11–13). 4PBA is mainly an ammonia scavenger, but it has also chaperone activity, since it interacts with hydrophobic domains of misfolded proteins favoring their folding (13). 4PBA also works as mild histone deacetylase inhibitor, promoting gene transcription (14).

TUDCA, the taurine conjugate form of ursodeoxycholic acid (UDCA), is a soluble bile acid and its main effect as chemical chaperone is based on improving protein folding capacity by activation of the unfolded protein response (UPR) sensor activating transcription factor 6 and by assisting the trafficking of mutant proteins. Furthermore, it inhibits the phosphorylation of eIF2a, a target of the UPR sensor protein kinase RNA-like endoplasmic reticulum (ER) kinase, responsible for inhibition of protein translation and apoptosis activation (15).

The *in vivo* evaluation of pharmacological treatments represents the most powerful and desirable approach in drug screening studies, since it allows consideration not only of the cell specific effects of the compound, but also its absorption, organ distribution, metabolism, excretion and toxicity in the whole organism. Of course, the availability of a valid model able to provide large dataset of results in short time and at low cost is a fundamental prerequisite. Murine models do not seem to satisfy such features due to the considerable effort required for their generation and validation, housing space and cost, amount of drugs necessary for the studies and number of animals to be sacrificed. Recently the small teleost *Danio rerio* stood up as a better choice for drug screening trials (16). *Danio rerio*, known as zebrafish, has been used extensively for genetic studies of vertebrate development due to its high fecundity, externally fertilization and embryo transparency. These characteristics, together with the high-quality genome sequence available (17,18), the generation of transgenic lines with fluorescent proteins expressed under cell/tissue specific promoters (19), the possibility to easily knock down genes by morpholino (20) and to generate mutant lines with the CRISPR/Cas 9 editing system (21), strongly expanded zebrafish use for the investigation of human diseases. Indeed, large-scale mutagenesis studies revealed that zebrafish reproduces many of the diseases described in tetrapods, including those affecting the skeletal system (22). Despite the evolutionary distance between humans and teleosts, zebrafish shares 82% of disease associated targets and a large number of drug metabolism pathways (17,23). In particular, considering the skeletal system, the gene expression profile associated with bone development is highly conserved between tetrapods and zebrafish. Moreover, the types of ossification, membranous and endochondral, as well as the presence of all the bone cell types are common to zebrafish and humans (24,25). Indeed multiple skeletal disorders have been recapitulated in zebrafish, including both dominant and recessive OI forms (22,26–29) and screening for anabolic bone compounds was previously successfully accomplished (30).

The use of zebrafish as a cheap and convenient tool for drug screening studies is further supported by the ability to administer most drugs in a small volume of water without need for invasive

procedures and to house zebrafish, at least in the larval stage, in multi-well plates suited for high-throughput analysis and automated screening (11,30).

A zebrafish model for the classical form of OI, named *Chihuahua* (*Chi*/+), was discovered as a result of a large N-ethyl-N-nitrosourea (ENU)-mutagenesis screening and identified by an X-ray-based screening aimed at recognizing abnormal skeletal patterning. *Chi*/+ carries in heterozygosis a typical glycine substitution (G574D, p.G736D) in the triple helical domain of the α1 chain of type I collagen, the most common cause of classical OI and revealed the bone outcome of severe human OI (22).

In the present study we performed the first deep investigation of *Chi*/+ fish from larval to adult stage validating it as a model for classical OI from a biochemical, morphological and cellular point of view. We confirmed the intracellular retention of mutant collagen causing ER enlargement in zebrafish and succeeded in ameliorating the outcome of OI by administration of 4PBA targeting osteoblasts malfunction.

Results

In order to use the zebrafish *Chihuahua* mutant for drug screening studies to discover novel OI therapies, a deep phenotypic characterization of larval and adult mutant fish was performed. Since OI is mainly associated with short stature, extreme bone fragility and skeletal deformity, these parameters were first investigated.

Adult *Chi*/+ fish are shorter and show deformed and fragile bones compared with WT

The growth of heterozygous *Chi*/+ and WT zebrafish was followed from 2 to 40 weeks post-fertilization (wpf) by measuring the standard length (SL) (Fig. 1A). Although *Chi*/+ fish were shorter than WT from 3 wpf, the difference was significant only starting from 18 wpf (*Chi*/+: 12.55 ± 2.45 mm, $n = 15$; WT: 15.34 ± 4.08 mm, $n = 12$; $P = 0.04$) and by 40 wpf the mutants were ∼70% the size of the controls ($P = 0.006$) (Fig. 1B). The gross *Chi*/+ outcome showed an abnormal body and head shape, thus morphometric measurements were performed. The height at anterior of anal fin (HAA), the distance from the snout to the most posterior point of operculum (SOL) and the ventral to dorsal head height (HE) were evaluated (Fig. 1A). At 18 wpf HAA was similar in *Chi*/+ and WT (2.82 ± 0.85 mm, $n = 15$ and 3.05 ± 0.95 mm, $n = 12$, respectively; $P = 0.51$), but the significant lower SL/HAA ratio (*Chi*/+: 4.60 ± 0.58 and WT: 5.13 ± 0.43; $P = 0.01$) confirmed a more stocky body shape in mutants with respect the WT. The SOL/HE ratio was also significantly smaller in mutant fish (*Chi*/+: 1.23 ± 0.05 and WT: 1.33 ± 0.09; $P = 0.001$) supporting a more flattened head. By 19 wpf the SOL was shorter in *Chi*/+ compared with WT (3.35 ± 0.61 mm and 3.92 ± 0.69 mm: $P = 0.032$).

The abnormal shape of the caudal fin, already described in (22), gave rise to a lower ratio between the longest and shortest tail axes in *Chi*/+ compared with control fish (Fig. 1C). The difference was detectable, although not significant, at 1 month post-fertilization (mpf; *Chi*/+: 1.50 ± 0.05, $n = 4$; WT: 1.52 ± 0.11, $n = 10$; $P = 0.66$), but significance was reached at 2 mpf (*Chi*/+: 1.64 ± 0.14, $n = 26$; WT: 1.85 ± 0.09, $n = 27$; $P < 0.001$).

Rib fractures and vertebral fusions were detected in adult *Chi*/+ fish by X-ray and confirmed by alcian blue/alizarin red staining (Fig. 1D and E). The skeletal specific staining allowed also a more detailed analysis of bone deformities. Vertebrae were clearly misshapen, with altered and highly irregular post-zygapophysis and prezygapophysis protrusions (Fig. 1E, ii). Ribs appeared twisted and misshapen, with numerous calli indicating the healing of spontaneously occurring fractures (Fig. 1E, i). Fin structure was seriously compromised as already reported by Duran *et al.* (31), in particular the pelvic fins appeared atrophic and twisted (Fig. 1E, iii and iv).

Also, the slope of the neural spine was altered in mutant fish. The mean of the neural spine slope of the 10 precaudal vertebrae (measured as described in Materials and Methods; Fig. 1E, ii) was steeper in *Chi*/+ compared with WT fish starting from 1 mpf (55.66° ± 6.52° and 49.69° ± 5.23°, respectively; $P < 0.001$; $n = 4$ in each group) and a significant difference was confirmed at 2 mpf (*Chi*/+: 57.57° ± 6.64°, $n = 5$; WT: 54.83° ± 5.34°, $n = 4$; $P = 0.04$).

A strong reduction of bone mineral density in mutant compared with WT fish ($n = 5$ for each genotype and time point) was demonstrated by μCT images performed at 3 mpf (Fig. 1F) and 10 mpf (data not shown).

In general, most of the analyzed parameters revealed a worsening of the mutant phenotype with age.

Similar size but delay in mineralization characterized *Chi*/+ larvae compared with WT

Starting from 5 days post-fertilization (dpf), the presence of a pronounced fin fold bending already described by Fisher *et al.* (22) distinguished *Chi*/+ from WT. The angle of the fin fold bending, measured as described in Materials and Methods (Fig. 2A), was significantly different between *Chi*/+ and WT (137.77° ± 13.91°, $n = 204$ and 177.12° ± 2.90°, $n = 217$, respectively; $P < 0.001$).

Vital calcein labelling of 5 dpf fish revealed a delayed vertebral ossification. The notochord ossification began with the third and fourth vertebral centra and spread as expected in the two directions both in control ($n = 78$) and in *Chi*/+ ($n = 96$) fish (Fig. 2B). Interestingly, while all WT larvae showed almost complete ossification of the third, fourth and fifth centra (c3, c4, c5), about 50% of the *Chi*/+ larvae showed no ossification of these bones (Fig. 2C).

Alcian blue and alizarin red staining of 11 dpf larvae confirmed a significant mineralization delay in *Chi*/+ cranial bones compared with WT ($n = 50$ and 65, respectively) (Fig. 2D). The mineralization of 5th ceratobranchial (5CB), cleithrum (CL) and notochord (NC) was considered as example of endochondral, membranous and perichordal bone ossification, respectively. Three classes of mineralization were identified, namely beginning/no mineralization, incomplete and complete, based on the level of alizarin red staining. A significant reduction of bone mineralization was detected in mutant fish compared with WT for 5CB ($P = 0.003$) and cleithrum ($P = 0.007$), the bones with mineralization type conserved in tetrapods. No difference was instead present for notochord ($P = 0.802$) (Fig. 2E; Supplementary Material, Table S1).

Type I collagen is overmodified in *Chi*/+ zebrafish

Acid soluble and pepsin digested type I collagen extracted from skin, scales and bone of adult *Chi*/+ showed broader and slightly slower bands of the α chains with respect to control fish in SDS-PAGE, indicating the presence of collagen overmodification, a typical OI feature (Fig. 3A).

We recently demonstrated that the normal type I collagen melting temperature (T_m) in zebrafish is ∼35 °C (32) Fig. S1, but the T_m of *Chi*/+ skin and bone type I collagen determined by

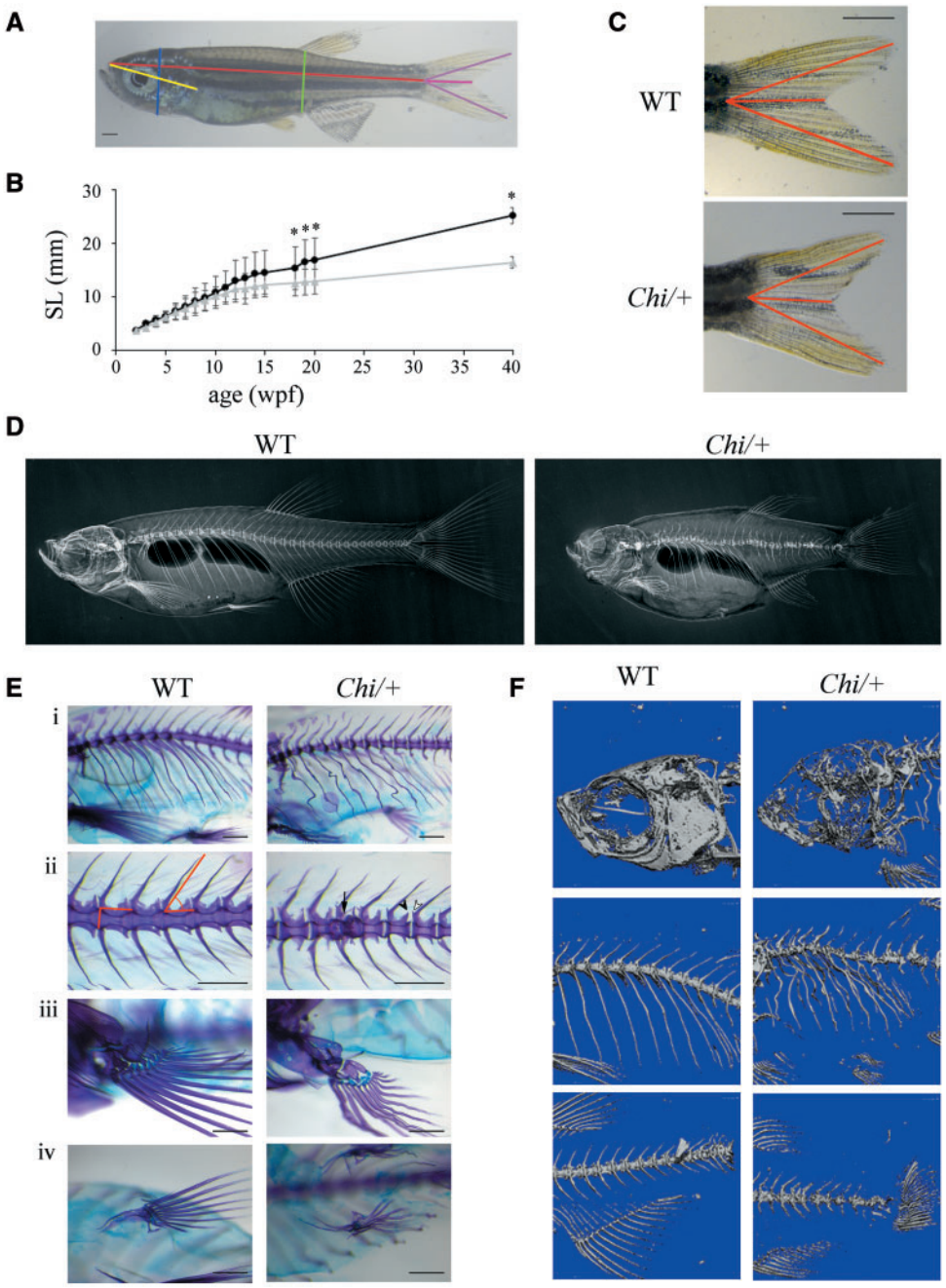

Figure 1. Morphological characterization of adult (*Chi*/+) zebrafish. **(A)** Morphometric parameters measured in adult fish. Standard length (SL) in red, height at anterior of anal fin (HAA) in green, height at eye (HE) in blue, snout-operculum length (SOL) in yellow, major axes of the caudal fin in purple, minor axis of the caudal fin in pink. **(B)** The growth curve shows that mutant fish ($n = 15$, grey triangles) are significantly smaller than WT ($n = 12$, black squares) from the 18th week post-fertilization (wpf). SL: standard length. $^*P < 0.05$. **(C)** Representative image of WT and *Chi*/+ caudal fin. The caudal fin of mutant fish has less pronounced lobes than the WT fin. The distances measured as described in Materials and Methods are highlighted in red. Scale bar: 1 mm. **(D)** WT and *Chi*/+ X-rays show severe alterations in the skeleton of mutant fish. **(E)** Skeleton magnifications of 3 months old WT and *Chi*/+ fish stained with alcian blue and alizarin red. Major and minor axes of the vertebral body and the slope of the neural spine are indicated (ii). Deformed ribs with bone calli (**i**), fused vertebrae (**ii**, arrow), misshapen prezygapophysis and post-zygapophysis (**ii**, white and black arrowheads), deformed pectoral (**iii**) and pelvic fins (**iv**) are evident in mutant fish. Scale bar: 500 μm. **(F)** μCT of 3 months old WT and *Chi*/+ fish reveals the severe under mineralization of mutant animals.

differential scanning calorimetry (DSC) showed a broad thermogram. The deconvolution of the curve resulted in three peaks, corresponding to a T_m of ∼35, ∼33 and ∼30 °C (Fig. 3B; Supplementary Material). Type I collagen melting temperature lower than normal is caused by abnormal protein structure and, based on these data, two populations of collagen molecules containing mutant chains seemed to be present in *Chi*/+ together with normal collagen. Interestingly, from the peak integration, the mutant collagen molecules corresponded to ∼ 33% of total collagen in bone (Fig. 3B) and ∼20–25% in skin (data not shown). This implies that limited amount of mutant collagen was incorporated in *Chi*/+ tissues.

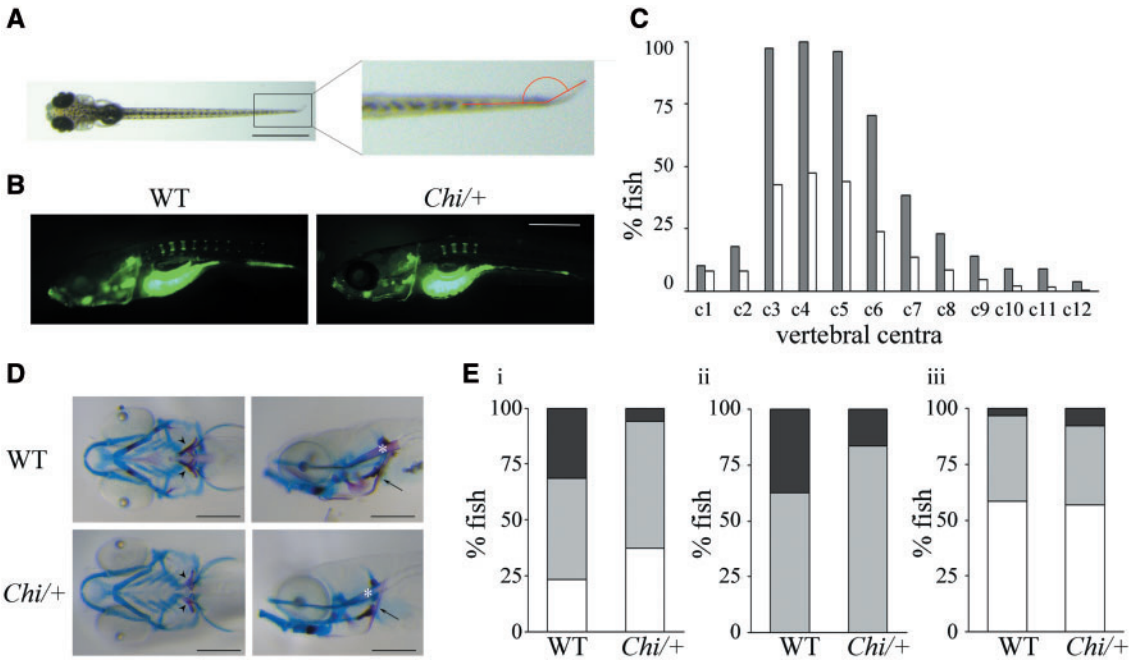

Figure 2. Skeletal evaluation of *Chi/+* larvae. **(A)** Fin fold angle is represented in red in 11 dpf fish. Scale bar: 1 mm. **(B)** Representative images of 5 dpf larvae WT and *Chi/+* stained with calcein. The delay in vertebral centra ossification is evident. Scale bar: 250 μm. **(C)** Percentage of 11 dpf fish presenting calcein positive (mineralized) vertebrae. c: vertebral centrum. Grey: WT; white: *Chi/+*. **(D)** Alcian blue and alizarin red staining of WT and *Chi/+* 11 dpf larvae in ventral and lateral orientation. 5th ceratobranchyal (5CB, arrowhead), cleithrum (CL, arrow) and notochord (NC, asterisk) are indicated. Scale bar: 200 μm. Delayed mineralization, represented by reduced alizarin red staining, is evident in the mutant larvae. **(E)** Percentage of 11 dpf WT and *Chi/+* larvae presenting distinctive levels of mineralization in the 5CB **(i)**, the CL **(ii)** and the NC **(iii)**. White indicates beginning/no mineralization, grey indicates incomplete mineralization and black indicates complete mineralization.

Enlarged ER in *Chi/+* fish

One of the typical features in OI patients and murine model type I collagen producing cells is the intracellular retention of the mutant protein associated with an enlargement of the ER cisternae and with cellular stress.

The easiest bone tissue to investigate in adult fish is represented by fin rays lepidotrichia, where it is relatively simple to identify in histological sections osteoblast lining cells of the hemi-rays. By transmission electron microscopy (TEM) we detected a general enlargement of the ER cisternae in adult *Chi/+* osteoblasts, absent in WT samples ($n = 5$ for each group) (Fig. 3C).

The presence of enlarged ER cisternae in mutant fish was also detected at embryo stage by injecting zebrafish embryos with the mRNA coding for a yellow fluorescent protein (YFP) targeting the ER. The percentage of embryos with strong intracellular fluorescent signal, supporting the presence of enlarged ER cisternae, was clearly higher in *Chi/+* (66.7%, $n = 9$) compared with WT (16.7%, $n = 12$) fish (Fig. 3D).

Increased Hsp47 expression in *Chi/+* compared with control larvae

Hsp47 is a fibrillar collagen specific chaperone known to assist procollagen assembly in the ER and its trafficking into the Golgi (33,34). As specific antibodies for zebrafish Hsp47 were not available, a rabbit was immunized with recombinant zebrafish Hsp47b lacking the ER retention signal. After affinity purification, the polyclonal antibodies specifically detected zebrafish Hsp47b (Supplementary Methods). Whole mount immunostaining using Hsp47b antibody on 5 dpf *Chi/+* ($n = 38$) and WT ($n = 36$) larvae showed a stronger signal in mutant compared with WT fish. A higher expression of Hsp47 in tail fin fold, skin and intersomitic space was evident in *Chi/+* compared with WT (Fig. 3E; Supplementary Material, Table S2).

4PBA ameliorates bone mineralization defect in *Chi/+* larvae

The enlarged ER detected in mutant *Chi/+* cells and the Hsp47 up-regulation prompted us to use the *Chi/+* model to target *in vivo* cellular stress as possible novel OI therapy. The administration of two different FDA approved molecules, 4PBA and TUDCA, known to act also as chemical chaperones was attempted. To determine the highest non-toxic dosage, toxicity tests at increasing concentrations were performed first. Doses of 0.05 mM for 4PBA and of 0.5 mM for TUDCA were chosen since they corresponded to the highest drug concentrations associated to normal phenotype at the end of the toxicity test (data not shown).

The period of treatment was selected based on the knowledge that at 11 dpf the organogenesis is completed and mineralization can be easily detected; furthermore, zebrafish can be kept in 96-well/plate limiting the drug requirement.

At the end of the treatment the fin fold bending and the mineralization level of 5CB, CL and NC in treated and untreated *Chi/+* and WT zebrafish were evaluated.

4PBA significantly increased the fin fold angle in *Chi/+* (treated: $145.99° \pm 13.58°$, $n = 192$; placebo: $137.77° \pm 13.92°$, $n = 204$; $P < 0.001$) (Fig. 4A). On the contrary, no significant effect was evident after TUDCA treatment (treated: $134.37° \pm 22.16°$, $n = 130$; placebo: $130.54° \pm 20.01°$, $n = 118$; $P = 0.16$), although after drug administration the caudal fin fold was slightly straightened (Fig. 4E).

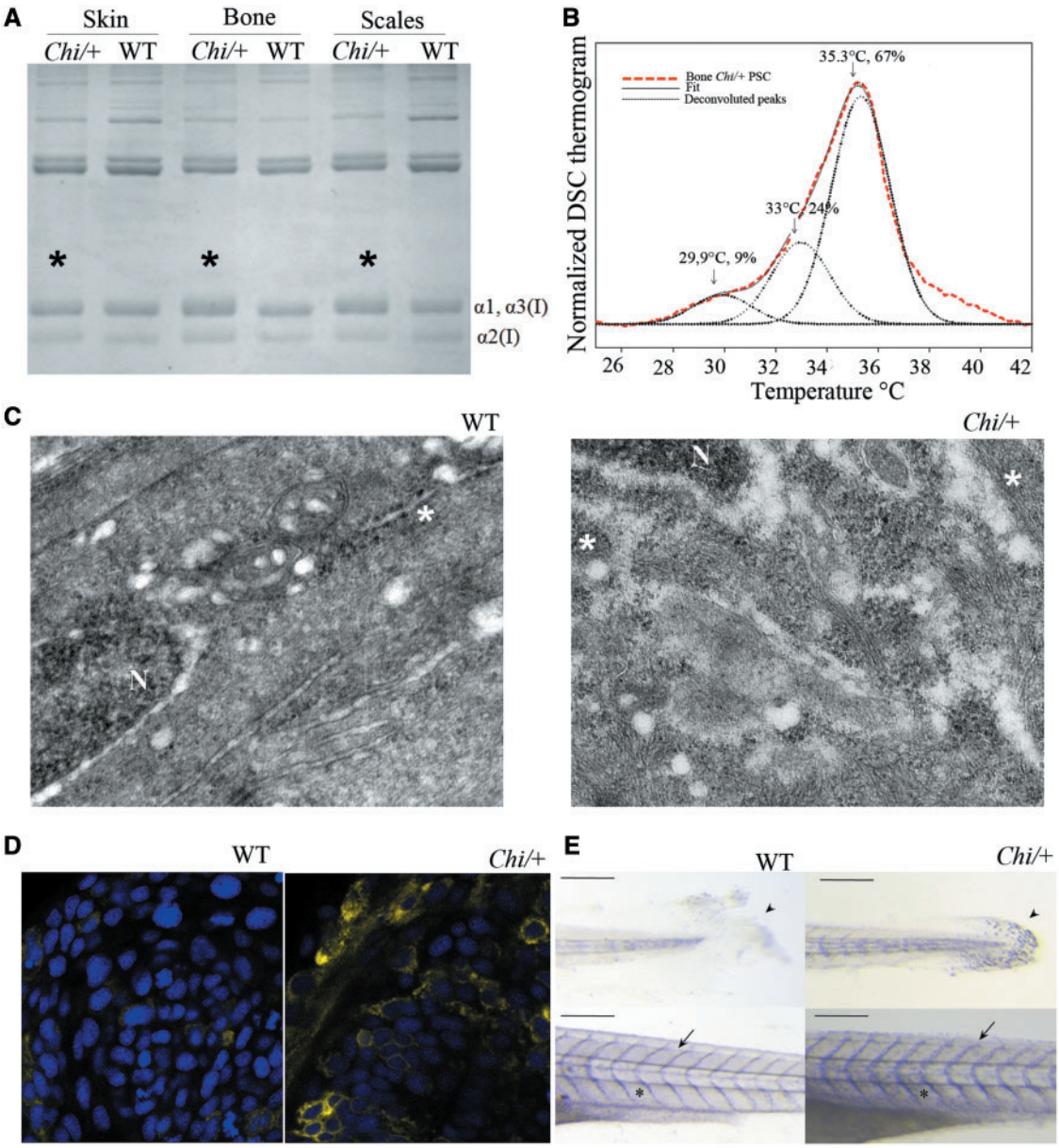

Figure 3. Biochemical and cellular evaluation of *Chi/+* collagen type I. **(A)** SDS-PAGE of collagen type I extracted from skin, bone and scales of WT and *Chi/+* adult fish. Mutant collagen is characterized by broader α bands (asterisks), indicating collagen type I overmodification. **(B)** Representative DSC thermogram of collagen extracted from bone of *Chi/+* adult fish. The presence of three melting temperature (T_m) peaks is evident from the deconvolution analysis of the thermogram. Similar result was obtained for collagen extracted from skin and scales (data not shown). **(C)** Transmission electron microscopy image of the caudal fin of WT and *Chi/+* adult fish. The enlargement of endoplasmic reticulum (ER) cisternae is evident in mutant fish. N: nucleus; *: rough endoplasmic reticulum (ER). Magnification 12000X. **(D)** Confocal microscopy images of 24 hpf embryos WT and *Chi/+* injected with mRNA expressing yellow fluorescent protein in the ER. A stronger signal in the mutant sample is demonstrated. Magnification 40X, zoom 4X. **(E)** Whole mount immunohistochemistry of 5 dpf WT and *Chi/+* embryos using Hsp47b antibody. A stronger signal is evident in tail, skin and intersomitic space in mutant larvae. Arrow: intersomitic space, arrowhead: tail; asterisk: skin. Scale bar: 200 μm.

Regardless the difference between the genotypes, 4PBA administration had a borderline significant effect on 5CB mineralization ($P = 0.07$), determining an overall 10% increment of the number of mineralized fish with respect the placebo group (Fig. 4B; Supplementary Material, Table S3). The effect of the treatment on 5CB mineralization was also explored within genotypes. 4PBA increased the complete mineralization in both WT and *Chi/+* with respect untreated fish, but the statistical relevance was not achieved (Supplementary Material, Table S4).

Similarly 4PBA significantly improved the mineralization of the NC ($P = 0.001$) (Fig. 4D; Supplementary Material, Table S3). This amelioration was evident in both genotypes, but the significance was detected only in WT ($P = 0.002$) (Supplementary Material, Table S4).

No 4PBA effect was detected on CL mineralization classes ($P = 0.424$) (Fig. 4C; Supplementary Material, Tables S3 and S4).

Mineralization analysis of treated and untreated mutant and WT fish did not reveal any significant difference following the TUDCA administration (Fig. 4F–H).

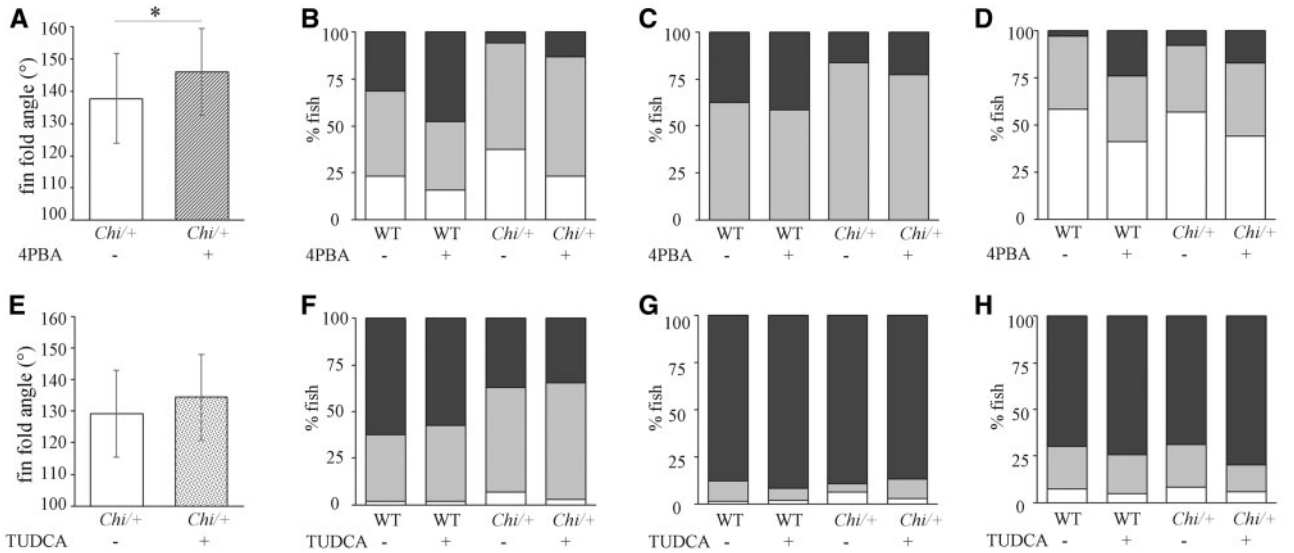

Figure 4. Effect of 4PBA and TUDCA treatment on *Chi/+* larvae. The caudal fin fold angle of 11 dpf *Chi/+* larvae increased after treatment with both 4PBA **(A)** and TUDCA **(E)**, but only 4PBA determined a significant straightening. $^{*}P < 0.001$. The administration of 4PBA increased the mineralization level of the 5CB **(B)**, CL **(C)** and NC **(D)** in mutant larvae. The treatment with TUDCA was ineffective in increasing the mineralization of all evaluated bones (CB, **F**; CL, **G** and NC, **H**) both in WT and in *Chi/+* larvae. In **(B)**–**(D)** and **(F)**–**(H)**, white boxes indicate beginning/no mineralization, grey boxes incomplete mineralization and black boxes complete mineralization.

Long-term 4PBA administration ameliorates skeletal phenotype in adult *Chi/+*

Based on the promising data obtained from the short term 4PBA administration to *Chi/+* larvae, mutant and WT fish were treated from 1 dpf to 3.5 mpf (WT: placebo $n = 18$, treated $n = 22$; *Chi/+*: placebo $n = 24$, treated $n = 21$). SL, tail shape and neural spine slope were evaluated at the end of the treatment.

The SL for both mutant and WT placebo was shorter than expected based on the growth curve values, in fact their size was compatible with 11 wpf animals. This was likely due to growing the zebrafish in bench tanks, the reduced water volume, the less controlled temperature and the limited food administration necessary to limit the water replacement. As expected a significant difference was not detected in the placebo groups (*Chi/+*: 10.40 ± 1.70 mm; WT: 11.37 ± 3.09 mm; $P = 0.40$), but 4PBA administration increased the *Chi/+* length to WT values (11.36 ± 2.11 mm and 11.55 ± 2.75 mm, respectively; $P = 0.77$).

The treatment normalized the mutant tail shape. The ratio between the longest and shortest tail axes (measured as reported in Materials and Methods and described in Fig. 1A) was significantly different in WT versus placebo mutant fish (1.77 ± 0.14 and 1.55 ± 0.10, respectively; $P < 0.001$), but it was increased in *Chi/+* after 4PBA treatment (*Chi/+*: 1.73 ± 0.25; $P = 0.08$), approaching the WT value (Fig. 5A).

The 4PBA also improved the morphology of the mutant skeleton. The slope of the neural spine in the precaudal vertebrae following drug administration was significantly reduced with respect untreated mutant fish ($50.69° \pm 7.86°$ and $53.06° \pm 8.19°$, respectively; $P = 0.002$), reaching the WT untreated value ($49.78° \pm 6.10°$) (Fig. 5B). The comparison performed on the single vertebral centra revealed that the most significant reduction of the slope was detected on the more caudal vertebrae analyzed (Supplementary Material, Table S5).

Mean vertebrae length and area were also increased significantly in *Chi/+* treated compared with the placebo group (length: 0.26 ± 0.06 mm and 0.22 ± 0.04 mm; $P = 0.04$; area: 0.045 ± 0.02 mm^2 and 0.034 ± 0.02 mm^2; $P = 0.047$).

4PBA treatment reduced ER cisternae size and increased the amount of extracellular collagen

In order to understand the mechanism of 4PBA in ameliorating the skeletal phenotype of *Chi/+* fish, TEM of 11 dpf 4PBA treated embryos was performed to investigate the ER cisternae size. Electron microscopy images revealed the presence of normal ER cisternae in treated *Chi/+*, although they were still coexisting with cisternae of enlarged size (Fig. 5C).

Whole mount immunostaining of 5 dpf treated and placebo *Chi/+* fish using Hsp47b antibody did not show any reduction in the expression of this type I collagen specific chaperone, that remains up regulated in mutant fish after treatment (Supplementary Material, Table S2).

Interestingly, more type I collagen was detected in mutant fish following 4PBA treatment, supporting an amelioration of its secretion. No such effect was detected following TUDCA administration. Taking advantage of the regenerative property of zebrafish tail, about half of adult *Chi/+* fish tail was cut and the secreted and newly deposited collagen was evaluated in absence or presence of 4PBA ($n = 3$ and 4, respectively) or TUDCA ($n = 4$ in each group) after 7 days. The higher percentage of fluorescent green signal in the regrown tails of 4PBA treated *Chi/+* zebrafish under polarized light after staining with picro sirius red clearly demonstrated an increased amount of collagen in the secreted matrix (Fig. 5D; Supplementary Material, Table S6). This increase was undetectable upon TUDCA administration (Supplementary Material, Table S7).

4PBA did not affect early and late osteoblast-specific genes expression

To evaluate if the inhibitory effect of 4PBA on class I and II histone deacetylases was affecting the transcription of bone forming cells specific genes, the expression of an early (*sp7*) and two late (*col1a1a* and *bglap*) osteoblast genes was evaluated by qPCR after 7 days of treatment in WT and *Chi/+* larvae. No difference

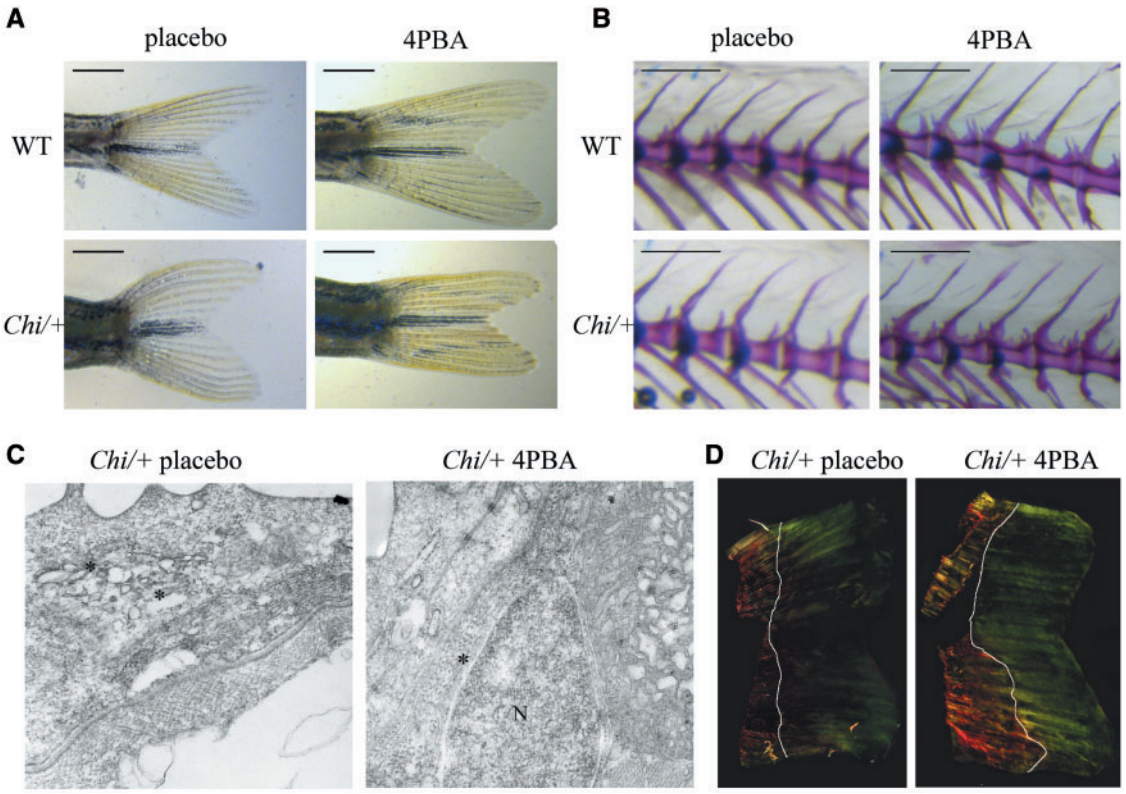

Figure 5. 4PBA treatment ameliorated the tail shape **(A)** and normalized the neural spine slope **(B)** of *Chi/+* fish after 14 weeks of treatment. Scale bar: 1 mm in **(A)** and 500 μm in **(B)**. **(C)** Transmission electron microscopy of 11 dpf *Chi/+* larvae showed a general reduction of the ER cisternae size after 4PBA treatment. Magnification 12000X. **(D)** Representative images of picro sirius red staining *Chi/+* zebrafish regrown tail after 7 days from tail clipping in absence or presence of 4PBA. A strongest signal in the sample obtained from 4PBA treated fish confirmed a higher amount of collagen in the matrix following 4PBA treatment. White lines indicate the portion of tail regrown in 7 days. Magnification 10X.

was detected for all of the three genes (Supplementary Material, Fig. S2A–C).

Western blot analysis using an antibody against acetylated-H3 did not reveal any significant difference in its expression following 0.05 mM 4PBA treatment in tissue lysates from larvae and adult fish (Supplementary Material, Fig. S2D and E), indicating that the inhibitory effect of 4PBA on histone deacetylases was not significant at the used concentration.

Discussion

With the ultimate aim to develop and validate a high throughput drug screening tool to find novel cure for the untreatable brittle bone disease OI, our study accomplished three major findings. First, the mutant zebrafish *Chihuahua* (*Chi/+*) was validated as model for classical OI by deep biochemical, morphometric and cellular characterization. Second, the power and advantages of this model for drug screening both in larvae and in adult were highlighted by defining easily traceable output. Finally, by a candidate approach 4PBA was identified to have potential to treat OI most likely based on its chaperone activity.

Chihuahua mirrored morphological, biochemical and cellular OI outcome

Short stature is a main hallmark for OI patients and small size is a common feature in OI murine models (2,6,8,35,36). The growth curve analysis performed from 2 to 40 wpf confirmed in *Chi/+* a growth delay together with a more stocky body and head shape compared with WT.

The two main biochemical properties of OI mutant type I collagen are excessive post-translational modification and reduced thermal stability due to altered structure (37,38). A slower and broader electrophoretic migration of α bands in type I collagen extracted from different *Chi/+* tissues supported the presence of overhydroxylated and overglycosylated protein also in this model. Furthermore, the T_m of type I collagen in mutant *Chi/+* was reduced. The DSC thermogram showed, together with the expected peak at ∼35 °C corresponding to the fraction of collagen molecules containing only normal α chains (32), two lower T_m peaks at ∼33 and ∼30 °C suggesting the presence of at least two different populations of collagen molecules with mutant ($\alpha1^{G574D}$) chains. In zebrafish, type I collagen may contain not only α1 and α2 chains, but also a third chain, namely α3, which is encoded by the *col1a1b* gene and absent in tetrapods (32,39). We recently proposed the presence of an equimolar amount of the three α chains in zebrafish type I collagen, leaving open the possibility of the existence of α1α3α2 alone or the presence of equal amounts of α1α1α2 and α3α3α2 or a combination of the three trimers (32).

Since only a single DSC peak with T_m ∼35 °C was observed in wild-type fish (Supplementary Material, Fig. S1), the additional DSC peaks of *Chi/+* bone collagen with T_m ∼33 °C and T_m ∼30 °C (Fig. 3B) likely represent the molecules with one and two $\alpha1^{G574D}$ chains, respectively (38). Based on our previous findings on zebrafish type I stoichiometry (32) the presence of $\alpha1^{G574D}\alpha1^{G574D}\alpha2$ trimers suggests that zebrafish collagen contains either all three

possible trimers or just α1α1α2 and α3α3α2, but not α1α3α2 alone. The observation of ∼33% mutant molecules in bone (Fig. 3B) and <25% mutant molecules in skin (data not shown), which are values lower than expected based on the proposed stoichiometry (Supplementary Material, Table S8), indicated either a low matrix incorporation for the mutant collagen or its partial intracellular retention.

Indeed enlargement of ER in *Chi*/+ mutant fish was demonstrated in fibroblasts by confocal microscopy and in osteoblasts by electron microscopy. Intracellular retention of mutant collagen has been widely demonstrated both *in vitro* and *in vivo* in OI patients and in murine models (35,40). The size of the ER correlates with the unfolded protein load and ER expansion is expected in presence of excessive misfolded proteins and it is normally associated to cellular stress.

Finally, whole mount immunohistochemistry on 5 dpf WT and mutant zebrafish revealed a strong Hsp47 signal in *Chi*/+ in the skin, in the space among somites and in the tail fin. An increased Hsp47 expression either at transcript or protein level, as well as an increased intracellular colocalization with mutant type I collagen, were reported in cells from OI patients and murine models (9,41). Hsp47 is an ER chaperone known to play a role in collagen synthesis by stabilizing the procollagen molecules. Hsp47 also facilitates type I collagen transfer from the ER to the Golgi compartment (33,34). An increased expression of Hsp47 in cells expressing structurally abnormal type I collagen may either represent an attempt to favor its proper synthesis and secretion and/or the impossibility for the mutant collagen to move properly throughout the secretory pathway.

Chihuahua: a zebrafish reproducing bone OI phenotype

μCT, X-ray and skeletal-specific staining confirmed the bone deformity and multiple rib fractures seen in adults *Chi*/+ zebrafish as originally reported (22), but also provided novel insight validating *Chi*/+ as good model for human OI. Furthermore, several vertebral compressions were identified both in abdominal and in caudal regions. Vertebral compressions associated with vertebral fractures are described in human OI and are mainly consequences of poor quality of bones that are unable to sustain the mechanical loading. Interestingly, none of the OI murine models reproduced the vertebral phenotype, mainly because rodents, as quadrupeds, have a structure of spine and center of gravity quite different from humans. Zebrafish instead bear cranial-to caudal spinal loads that are originated by swimming forward through water coupled with caudal propulsion and that are quite comparable to the gravitational load to which humans are subjected. Overall, the similar biomechanical forces along the spine seem to make fish more susceptible to vertebral damage (42) and thus a better model for mimicking human spine defects.

Vertebrae distortion was also detected in mutant fish, as demonstrated by a steeper slope of the neural spines compared with WT. The presence of mutant collagen in *Chi*/+ could be responsible for the deformity, since neural and haemal appendices are intramembranous bones and the lack of cartilage anlage underlines a relevant role for type I collagen in shape and mineralization of these structures (43).

Duran *et al*. described the presence of abnormal actinotrichia and lepidotrichia shape and length during fin development and regeneration in *Chi*/+ zebrafish (44). Actinotrichia are the first fin skeletal structures formed during development and they represent a support and a scaffold for the migration of mesenchymal stem cells responsible for the generation of the fin fold connective tissue (45,46). They consist of collagen fibrils mainly composed of a specific type of collagen II and of homotrimeric collagen I. The presence of abnormal actinotrichia in *Chi*/+ zebrafish underlined the importance of structurally correct collagen molecules for proper fin formation.

The significant reduction of the ratio between long- and short-tail axes in *Chi*/+ adults allowed us to quantify this abnormality originally reported by Fisher (22).

A significantly less acute angle of the *Chi*/+ larvae fin fold compared with WT was detected. It is interesting to notice that up to 3 dpf *col1a1a*, encoding for the α1 chain of type I collagen, is the only type I collagen coding gene that is expressed in the fin fold (31). Therefore, the change in the angle may either be the consequence of the presence of mutant protein and/or its reduced amount due to possible intracellular retention as discussed in following sections.

Of note, although no size difference could be detected at larval stage in mutant *Chi*/+ compared with WT, as previously reported, a delay of mineralization was detected at the level of 5th ceratobranchial, cleithrum and notochord tip, examples of endochondral, membranous and perichordal bones. Delayed mineralization is another common feature in OI, reported for several OI murine models (47) and is known to affect both membranous and endochondral bones (48).

4PBA administration ameliorated the bone phenotype in *Chi*/+ larvae and adults acting mainly as chemical chaperone

A definitive cure for OI will require the correction of the genetic defect, and although gene therapy approaches are under investigation, the bench to bed transition of such strategies is far in time (49–51). In the last years drug repositioning approach demonstrated to be an elective choice for disease treatment based on economic and timing reasons and it is definitely appealing for rare disorders (10). The identification of curative effect of molecules already approved by FDA will bypass at least some of the more expensive and time consuming phases for drugs development.

The availability of a validated zebrafish model for classical OI motivated our study on this direction.

Based on recent findings, the outcome of OI and of other skeletal disorders associated with misfolded structural proteins partially retained inside the cells is not only due to abnormal extracellular matrix, but also to altered cellular homeostasis. Thus, targeting cellular stress could represent a valid approach to ameliorate the disease phenotype (52–54).

For our study, we treated the OI zebrafish model *Chi*/+ with 4PBA and TUDCA, already approved by the FDA for urea cycle disorders and cholestasis respectively and known to have chaperone activity (11,12). Their administration was facilitated by the fact that they are water soluble molecules.

Only 4PBA significantly improved straightening of the fin fold in mutant larvae and rescued the mineralization delay in *Chi*/+ zebrafish. Although significant values were not always reached, a clear tendency to higher mineralization was detected in 5CB and NC of treated WT and mutant fish. Furthermore, a long-term treatment with 4PBA from 1 dpf to 3.5 mpf resulted in an amelioration of growth, vertebral shape and tail symmetry.

We first evaluated the effect of the drugs at larval stage taking advantage of the small amount of the required drug and the space for husbandry. For the evaluation of drug efficacy, the fin

fold bending characteristic of the *Chi/+* model, most likely associated to the presence of mutant type I collagen, was first determined. The small fin fold phenotype and/or abnormal tail shape is a common feature in various zebrafish models of skeletal diseases caused either by the absence or the presence of mutant structural proteins (44,55,56). The most abundant structural elements in the early fin fold and in the distal region of adult tail are actinotrichia, structures containing both collagen I and collagen II (31). Collagen IX is known to interact with collagen II and to have a role in vascular plexus formation in caudal fins. A mutation in *col9a1* is present in the *persistent plexus* (*prp*) zebrafish mutant. Interestingly, overexpression of *col9a1* in *prp* ameliorates the fin fold phenotype, supporting the idea that also increasing the amount of structurally abnormal protein in extracellular matrix may lead to an amelioration of the phenotype (56). This is reminiscent to what was observed in OI patients and murine models following bisphosphonate treatment, leading to reduced bone turnover and consequently to an increase of collagen I content in the bone matrix.

Type I collagen is the major organic component of bone and its amount is strictly linked to bone mineral density (57). Using TEM analysis in zebrafish larvae and a tail fin regeneration assay in adults we demonstrated that the amelioration of the bone phenotype in *Chi/+* after administration of 4PBA is caused by an increase of collagen secretion associated to a reduction of ER cisternae size due to the chaperone function of the drug. TEM showed a partial rescue of the ER cisternae enlargement, showing a prevalence of normal size cisternae in larvae grown in the presence of 4PBA and picro sirius red staining of the regenerated tail in 4PBA treated mutant fish revealed an increase in collagen amount.

The intracellular collagen folding requires specialized chaperones (i.e. PDI, FKBP65, HSP47) (58) and it seems unlikely that the small 4PBA molecule could mimic such a complex group of proteins. It may be possible that 4PBA interacts with hydrophobic unfolded regions of the triple helix and limits the intracellular aggregation of mutant collagen favoring its secretion and maybe limiting its degradation (59,60). However, we cannot exclude that 4PBA acts intracellularly on non-collagenous proteins whose folding and secretion may be compromised by the flooding of the ER.

Since 4PBA is also known to act as a mild inhibitor of histone deacetylase, such a role was further investigated.

The culture of osteoblasts in the presence of Na-butyrate was reported to increase histone acetylation, to stimulate cell proliferation, and to promote osteoblast maturation by favoring *Runx2* expression (61). The presence of Na-butyrate stimulated alkaline phosphatase activity in murine calvarial organ cultures (62).

To date little *in vivo* data exist that suggest a dose dependency of 4PBA for the inhibition of histone deacetylase and/or its chaperone function. Luo *et al*. demonstrated that intraperitoneal injection of 4PBA 20 mg/kg/day for 4 weeks was enough to attenuate ER stress in a murine model of myocardia hypertrophy, whereas a 100 mg/kg/day was necessary to inhibit histone deacetylases (63). On the other hand, a single injection of 10 mg/Kg was sufficient to protect mice from radiation preserving histone H4 acetylation (64).

Based on existing *in vitro* and *in vivo* data and considering that, at least for some drugs the micromolar doses in zebrafish are comparable to milligrams per kilograms in mice (65), the 4PBA concentration used in our study should not significantly inhibit histone deacetylase activity.

Indeed distinct difference in expression of acetylated histone 3 was not detected at protein level in 11 dpf 4PBA treated larvae as well as in tail extracts from adult treated zebrafish. Similarly, no difference in the transcription of bone markers was detected by qPCR.

The lack of effect following TUDCA administration is not unexpected. The two molecules are chemically different and they can act in different ways, as already reported (66,67). Furthermore, we cannot exclude a yet unknown contribution of 4PBA for bone homeostasis.

In conclusion, we reported a comprehensive investigation of the *Chi/+* zebrafish OI model validating it as a powerful tool for study OI pathophysiology. We identified peculiar phenotypic outcomes that could be easily used as tools to validate the efficiency of molecules in high throughput drug screening tests. 4PBA was demonstrated to be a promising candidate for OI due to its chaperone activity.

Materials and Methods

Husbandry

Wild-type AB (WT) and heterozygous *Chihuahua* (*col1a1a*$^{dc124/+}$, *Chi/+*) zebrafish arise from natural spawning or from *in vitro* fertilization. The mutant *Chi/+*, provided by Professor Shannon Fisher (Dept of Pharmacology & Experimental Therapeutics, Boston University School of Medicine, USA), carries a G2207A mutation in *col1a1a*, causing a p.G736D (G574D) substitution in the α1 chain of type I collagen. Embryos were kept in Petri dishes in fish water ($NaHCO_3$ 1.2 mM, instant ocean 0.1 g/L, $CaSO_4$ 1.4 mM, methylene blue 0.00002% w/v) at 28 °C until 6 day post-fertilization (dpf), then housed in ZebTEC semi-closed recirculation housing systems (Tecniplast) and kept at a constant temperature (27–28 °C), pH (7.5) and conductivity (500 μS) on a 14/10 light/dark cycle. For the experiments stated below larvae and adult fish were anesthetized using a solution of tricaine (3-amino benzoic acidethylester, Sigma Aldrich) 0.0016% w/v, in fish water and sacrificed by tricaine overdose (0.03% w/v). All experiments were performed in accordance with the approved guidelines, in agreement with EU Directive 2010/63/EU for animals. The experimental protocol was approved by the Italian Ministry of Health (Approval Animal Protocol No. 1/2013).

Genotyping

Depending on the experiment type, DNA was extracted from single embryos, pool of embryos or caudal fin biopsies from adult zebrafish. Tissues were lysed in Tris–HCl 100 mM, pH 8.5, EDTA 5 mM, SDS 0.2% w/v, NaCl 200 mM and proteinase K (Sigma Aldrich) 2.5 mg/ml, for at least 3 h at 55 °C. DNA was precipitated with isopropanol and dissolved in Tris–HCl 20 mM, EDTA 1 mM, pH 8.0. The *Chi/+* genotype was evaluated by PCR amplification of *col1a1a* (NC_007114.6) followed by restriction enzyme digestion. The following primers were used: sense 5'-TCTTAAGGGT GACAGAGTGAGTATGAC-3' (23101253–23101279) and reverse 5'-CAACTTCAAGATGTTTCATCACTTAGTATG-3' (23101543–2310 1514). Since the mutation creates a novel BtsCI restriction site, the amplicon was digested with this enzyme (New England Biolabs) and the products separated on 2% agarose gel. A single 290 bp band revealed the presence of the WT allele, while the mutant allele generated 141 and 149 bp fragments.

Morphometric evaluation

Zebrafish were anesthetized with tricaine and images were acquired with a Leica M165 FC microscope (Leica) connected to a

Leica DFC425 C digital camera (Leica). Measurements were performed using the Leica LAS v4.5 software (Leica).

The fin fold angle was measured on dorsal images of 11 dpf zebrafish as the angle between the notochord axis and the line connecting the posterior tip of the notochord and the terminal end of the fin (Fig. 1A).

Using lateral images of embryos and adult fish the following parameters were measured: SL, defined as the distance from the snout to the caudal peduncle or, in pre-flexion larvae that do not have a caudal peduncle, to the posterior tip of the notochord; HAA, defined as the distance from ventral to dorsal, measured immediately anteriorly to the anal fin and perpendicularly to the axis defined by SL; Snout-Operculum Length (SOL), defined as the distance from snout to the most posterior point of operculum; height at eye (HE), defined as the distance from ventral to dorsal, measured immediately posteriorly to the eye and perpendicularly to the axis defined by SL (68) (Fig. 1A). The symmetry of the tail was evaluated as the ratio between the mean of the two major axes (defined as the distance between the central part of the caudal peduncle and the tip of each caudal lobe) and the minor axis (the distance between the central part of the caudal peduncle and the conjunction point of the two caudal lobes) of the tail (Fig. 1A and C).

The shape and the size of vertebrae were evaluated on images of adult fish stained with alcian blue and alizarin red acquired on lateral orientation. For the dimension, the major and the minor axis of each vertebra were defined respectively as the mean of the length measured dorsally and ventrally and as the mean of the height measured anteriorly and posteriorly to the vertebral centrum (Fig. 1E, ii). The slope of the neural spine is measured as the angle between the major axis and the line connecting the edge of the spine with the most anterodorsal region of the centrum (Fig. 1E, ii). The first 10 vertebrae articulated with the ribs were considered.

Growth curve determination

WT and *Chi*/+ zebrafish were collected from *in vitro* fertilization and genotyped at 6 dpf based on the caudal fin fold curvature. Lateral images of each fish were acquired every week from 11 until 137 dpf and at 280 dpf. SL was measured as described above.

X-ray

X-rays of adult 3.5 months old fish were acquired with a Faxitron Mx-20 (Faxitron), using 25 kV for 10 s. The Kodak DirectView Elite CR System and k-Pacs software (Kodak) were used.

μCT

WT and *Chi*/+ zebrafish at 3 ($n = 5$ and 6, respectively) and 10 mpf ($n = 5$ for both genotype) were sacrificed, fixed overnight at 4 °C in paraformaldehyde (PFA) 4% (w/v) and stored in ethanol 75% v/v. For μCT fish were placed in a radiotranslucent sample-holder, foam pads were applied to prevent shifting during the scan process and the specimens were scanned with a μCT 40 desktop cone-beam μCT (Scanco Medical) using a voxel size of 10 μm with 1000 projections per slice at a tube energy of 55 kV with an intensity of 145 μA. Reconstructed slices were segmented using the script 'UCT_EVALUATIONV6' of the Scanco MicroCT software suite with the following parameters: sigma = 0.8; support = 1; lower = 165–185; upper = 1000; unit = 6. The lower threshold was varied between 165 and 185 to provide the optimal signal/noise ratio for each sample. Three-dimensional reconstructions were imaged using the program μCT Ray V3.8 of the Scanco MicroCT software suite.

Skeletal staining

Cartilage and bone were stained with alcian blue and alizarin red using a protocol modified from Walker *et al.* (69). Both larval and adult WT and *Chi*/+ zebrafish were sacrificed and fixed overnight in PFA 4% w/v in PBS (Sigma Aldrich) with $CaCl_2$ 0.9 mM and $MgCl_2$ 0.49 mM, pH 7.4 at 4 °C. Scales and internal organs were manually removed from adults, and fat was eliminated by an overnight bath in acetone. Embryos and adult fish were stained overnight at room temperature (RT) with a solution of alcian blue 8GX (Sigma Aldrich) 0.02% w/v, ethanol 70% v/v, $MgCl_2$ 80 mM and then rehydrated in a series of ethanol (80, 50, 25%), in Tris–HCl 100 mM, pH 7.5, $MgCl_2$ 10 mM, 5 min each. Bleaching to eliminate the pigmentation was performed with H_2O_2 3% v/v, KOH 0.5% w/v at RT and followed by two washes in glycerol 25% v/v, KOH 0.1% w/v. Soft tissues were digested with 1 mg/ml (for larvae) or 10 mg/ml (for adult fish) trypsin dissolved in a 30% v/v, solution of saturated $B_4Na_2O_7$ for a time depending on fish size. After the staining in alizarin red S (Sigma Aldrich) 0.01% w/v, glycerol 25% v/v, Tris–HCl 100 mM, pH 7.5 overnight at RT, fish were washed in increasing glycerol/KOH 0.1% series (50%, 80%) and finally stored at 4 °C in glycerol 100%, KOH 0.1%. Images were acquired using a Leica M165 FC microscope connected to a Leica DFC425 C digital camera. The mineralization of the 5th ceratobranchial, the notochord and the cleithrum was evaluated. Three operators blinded to the genotype of the fish qualitatively described the level of ossification of these bones for each embryo as beginning/no ossification, intermediate ossification or complete ossification independently.

Calcein ($C_{30}H_{26}N_2O_{13}$, Sigma Aldrich) was used as vital dye to stain calcified bones. WT and *Chi*/+ 5 dpf zebrafish were transferred to a physiologic solution (NaCl 0.9% w/v, pH 7.5) containing calcein 0.2% w/v for 20 min, washed with fish water until water was clean and kept in clear water overnight. The day after animals were anesthetized with tricaine and mounted in methylcellulose (Sigma Aldrich) 3% w/v. Fish images were acquired as previously described using a GFP filter. Three operators blinded to the genotype of the fish evaluated the ossification of the centra independently.

Type I collagen analysis

Bones (vertebrae, ribs and head bones), scales and skin were dissected from adult mutant and WT fish following sacrifice. The tissues were defatted for 6 h in NaOH 0.1 N at 4 °C. The scales and bones were decalcified for 48 h in EDTA 0.5 M pH 7.4 at 4 °C. The acid-soluble type I collagen (ASC) was obtained by protein extraction in acetic acid 0.5 M at 4 °C for 48 h. The ASC was then precipitated by NaCl 0.9 M in acetic acid 0.5 M. The pepsin-soluble fraction (PSC) was obtained by further digestion of the pellet obtained from the acetic acid extraction with pepsin 0.1 mg/ml in acetic acid 0.5 M at 4 °C for 48 h. The PSC was precipitated by NaCl 0.9 M in acetic acid 0.5 M overnight at 4 °C. Both ACS and PSC fractions were quantified by measuring the 4-hydroxyproline amount after acid hydrolysis. The purified collagen was analyzed on 6% polyacrylamide gel electrophoresis (SDS-PAGE) in the presence of urea 0.5 M. The gels were

stained overnight with picric acid 0.08 M, Coomassie Brilliant Blue R250 (Sigma Aldrich) 0.04% w/v destained in tap water and acquired with Versadoc3000 (BIO-RAD).

Differential scanning calorimetry

DSC thermograms of collagen solutions in HCl 2 mM, pH 2.7 were recorded in an N-DSC III differential scanning calorimeter (Calorimetry Sciences Corporation) at 0.25 °C/min heating rate.

Transmission electron microscopy

Following anesthesia in 0.0016% tricaine the caudal fin biopsies were obtained from adult WT and *Chi*/+ fish and rapidly transferred in Karnowsky fixative (sodium cacodylate 0.1 M, pH 7.8, glutaraldehyde 1.5% v/v, paraformaldehyde 4% w/v) overnight at 4 °C. Samples were then decalcified in EDTA 14% w/v pH 7.1 at 4 °C, for 24 h for *Chi*/+ and 48 h for WT. *Chi*/+11 dpf embryos treated with placebo or 4PBA were sacrificed with 0.03% tricaine and fixed with Karnowsky fixative overnight at 4 °C. The samples were then post-fixed in OsO_4 2% w/v in H_2O for 2 h at RT, rinsed in distilled water and dehydrated in ethanol. The specimens were infiltrated with LR White acrylic resin overnight at 4 °C and polymerized in gelatin capsules at 60 °C for 24 h. Thin sections (60–70 nm thick) were cut on a Reichert OM-U3 ultramicrotome with a diamond blade and collected on 300-mesh nickel grids. The grids were finally stained with saturated acqueous uranyl acetate followed by lead citrate and observed with a Zeiss EM900 electron microscope, operated at 80 kV with an objective aperture of 30 μm.

Confocal analysis of embryos

The ER-YFP vector (by courtesy of Yung-Yao Lin of the Wellcome Trust Sanger Institute, Hinxton, Cambridge, UK) which encodes a fluorescent fusion protein carrying calreticulin ER targeting and lysine–aspartate–glutamate–leucine retrieval sequences was used to analyze ER morphology (70). The mRNA was *in vitro* transcribed from the linearized construct using the mMACHINE mMESSAGE kit (Ambion) according to the supplier's instructions. The RNA integrity was verified on denaturing 1% agarose gel and the RNA clean-up and concentration was performed using the RNeasy MiniElute Cleanup kit (QIAGEN). The ER-YFP RNA was microinjected into embryos at the stage of 2–4 cells, using 300 pg of RNA and dextran conjugated with Alexa 647 (Molecular Probes) 0.05% w/v as tracer in a total volume of 4 nL for each injection. Microinjection was carried out using an InjectMan micromanipulator (Eppendorf) assembled on a Leica M165 FC stereomicroscope. At 24 hpf, the chorion was manually removed and the embryos fixed in PFA 4% w/v overnight at 4 °C. The samples were permeabilized with PBS containing Triton X-100 (BDH Chemicals) 0.1% v/v, in ice for 10 min, and stained with 4',6-diamidino-2-phenylindole (DAPI, Sigma Aldrich) 100 ng/ml for 30 min. The embryos were cut in half: the tail was mounted on a cover slip in 30 μL of 1% low melting agarose at 60 °C to be analyzed at confocal microscopy (TCS SP2-Leica), while the head was used for genotyping. The fluorescence intensity was qualitatively evaluated by three independent operators blinded to the fish genotype. The results were expressed as percentage of fish with brighter signal.

Picro sirius red collagen staining

The caudal fin of adult *Chi*/+ zebrafish was cut and either treated with 4PBA ($n = 4$), or TUDCA ($n = 4$) or with placebo ($n = 3$ for 4PBA experiment, $n = 4$ for TUDCA experiment) for 7 days. Then, the regrown caudal fins were cut again and fixed overnight in PFA 4% w/v in PBS. Tails were stained 1 h in Sirius Red 0.1% w/v (Direct Red 80, Sigma Aldrich) in saturated aqueous solution of picric acid (Sigma Aldrich). After the staining tails were washed in acetic acid 0.5% v/v, and directly dehydrated three times in absolute ethanol. Samples were clarified with xylene and mounted with DPX (Sigma Aldrich). Slides were observed under polarized light with the LEICA DM2500 microscope (Leica) and acquired using the LEICA ICC50 W digital camera (Leica). The analysis of the total and the green area were performed using Leica LAS4.5 software.

Whole mount immunostaining

4PBA treated (WT $n = 26$, *Chi*/+ $n = 24$) and untreated (WT $n = 36$, *Chi*/+ $n = 38$) zebrafish embryos were collected at 5 dpf, fixed overnight in PFA 4% w/v in PBS., washed in PBS and permeabilized overnight in methanol at −20 °C. Samples were hydrated with ethanol (100, 80, 70, 50, 0%) in PBS and digested with proteinase K 0.1% w/v in PBS at 25 °C for 15 min and hyaluronidase 2% w/v in PBS at 25 °C for 20 min. Embryos were fixed in PFA 4% for 30 min and PFA was eliminated by incubating samples with NH_4Cl 50 mM in PBS, for 1 h at RT. To block endogenous peroxidase activity embryos were incubated with bovine serum albumin (BSA, Sigma Aldrich) 0.5% w/v and H_2O_2 0.5% v/v, for 30 min at RT. After a 5 min wash with PBS, Tween-20 0.05% v/v (Sigma Aldrich) (PBS-T), blocking solution (BSA 5% w/v in PBS-T) was added for 2 h at RT. Hsp47b affinity purified antibody (1:1000 in 5% BSA/PBS-T) and anti-rabbit secondary antibody (1:200 in 1% BSA/PBS-T) were used. DAB substrate (Thermo Scientific) was finally added until appearance of the staining. Fish were incubated in increasing glycerol series (50%, 80%) and finally stored at 4 °C in glycerol 100%. Images were acquired using a Leica M165 FC microscope connected to a Leica DFC425 C digital camera. Three operators blinded to the genotype and the treatment of the fish evaluated presence or absence of the signal independently.

Drug toxicity test

Toxicity tests were performed to determine the relevant drug dosage. WT embryos (10 per group) were manually dechorionated at 24 hpf and treated from 1 to 7 dpf with different concentrations of the drug dissolved in fish water (0.05, 0.1, 0.5, 1, 5 and 10 mM for 4PBA (Sigma Aldrich), and 0.05, 0.1, 0.2, 0.5 and 1 mM for TUDCA (Sigma Aldrich) or with placebo in 96-well plates, using 200 μl per fish. Half of the volume was replaced with fresh solution every day. The number of surviving and the number of misshaped zebrafish were evaluated at the end of the treatment, in order to define the highest concentration without visible side effects.

Drug treatment

WT and *Chi*/+ embryos were obtained by *in vitro* fertilization, manually dechorionated at 24 hpf, and grown in 96-well plates (1 fish per well). 200 μl/embryo water per embryo with or without 4PBA 0.05 mM or TUDCA 0.5 mM were added starting from 1 dpf to 11 dpf. Half of the volume was replaced with fresh

solution every day. At 11 dpf fish were anesthetized with tricaine and lateral images were acquired using a Leica M165 FC microscope connected to a Leica DFC425 C digital camera. The caudal fin fold angle was evaluated, as described above, and used for genotyping. The fish collection mode varied based on the different experiments as detailed below.

For the long-term treatment, 4PBA was dissolved in water as described above for embryo treatment, and then larvae were transferred into tanks filled with 200 ml system water. Half of the volume was replaced every day with fresh solution, and fish were fed as described. The animals were sacrificed at 3.5 months. Digital images and X-ray were acquired. Then the fish were fixed in 4% PFA w/v in PBS for alcian blue and alizarin red staining. Morphometric analysis and mineralization level of 5th ceratobranchyal, cleithrum and notochord were performed as described above.

Western blot

4PBA treated or untreated mutant and WT 11 dpf embryos (4 for each genotype and treatment) were pooled and proteins were extracted using 20 μl of RIPA buffer (Tris–HCl 10 mM, pH 7.6, EDTA 5 mM, pH 8.0, NaCl 140 mM, NP40 0.5% v/v) added with protease inhibitors (EDTA 1.52 mg/ml, benzamidine 1.57 mg/ml, N-etilmaleimide 0.25 mg/ml, phenylmethylosulfonylfluoride 1 mM). 3.5 mpf WT and *Chi*/+ 4PBA treated and untreated fish caudal tails were cut, lysed in 100 μl/tail RIPA buffer containing protease inhibitor and sonicated 5 times for 10 s. Samples were centrifuged at 17 000*g* for 30 min, at 4 °C to remove cellular debris.

Proteins from two embryos or one tail were dissolved in Laemmli buffer with dithiothreitol 100 mM, denaturated for 10 min at 90 °C, separated in SDS-PAGE on a 15% polyacrylamide gel and transferred to a PVDF (GE Healthcare) membrane. Membrane was blocked with BSA 5% w/v in PBS with Tween-20 0.05% v/v (Sigma Aldrich) (T-TBS) and incubated with primary polyclonal Acetyl-Histone H3 (Lys9) antibody (Thermo scientific, J.942.2) diluted 1:1000 in BSA 5% w/v in T-TBS or with primary polyclonal actin antibody (1–19) (Santa Cruz Biotechnology, sc-1616) diluted 1:1000 in 2% w/v BSA in TBS-T overnight at 4 °C. Donkey anti-rabbit IgG-HRP antibody (Santa Cruz Biotechnology, sc-2077) or donkey anti-goat IgG-HRP antibody (Santa Cruz Biotechnology, sc-2020) were used as secondary antibodies both diluted 1:10 000 in BSA 2% w/v in TBS-T, 1 h at RT. ECL Prime Western Blotting Detection Reagent (GE Healthcare) was used for signal detection, membranes were acquired with Image Quant LAS4000 (GE Healthcare) and analysed using Image Quant TL (GE Healthcare) software.

qPCR

4PBA treated or untreated mutant and WT 11 dpf embryos were pooled ($n = 20$ for each group, 3 groups for each genotype and treatment) and RNA was extracted with Qiazol (Qiagen) following manufacturer's instructions. RNA quantity was determined with NanoDrop spectrophotometer and RNA quality by agarose gel electrophoresis. cDNA was synthesized from 1 μg of RNA using the High Capacity cDNA Transcription kit (Applied Biosystems) according to the manufacturer's protocol in a final volume of 20 μL.

qPCR was performed in 25 μL with SYBR Select Master Mix (Applied Biosystems) using the Mx3000P thermocycler (Stratagene) and the MxPro software (Stratagene). The following primers were used: for *col1a1a* (NM_199214.1) 5'-GAGT GATGGGTGCTATTGG-3' (1748–1766) and 5'-GGAATCCTCTG TCACCTCTA-3' (1996–1977); for *bglap* (NM_001083857.3) 5'-TG ACGTGGCCTCTATCATCA-3' (163–182) and 5'-TTTATAGGCGG CGATGATTC-3' (316–297); for *sp7* (NM_212863.2) 5'-GCTCCAA TCTTCACAGCACA-3' (944–963) and 5'-GCTGTGGACAGGTTTCTT CC-3' (1166–1147); for *actb1* (NM_131031.1) 5'-GAAGGAGATCACC TCTCTTGCTC-3' (995–1017) and 5'-GTTCTGTTTAGAAGCACTTC CTGTG-3' (1188–1164). The annealing temperature was 58 °C for *bglap* and *sp7* amplification and 60 °C for *col1a1a*. ΔΔCt method was used to compare gene expression in the different samples.

Statistical analysis

All values are expressed as mean ± standard deviation. The WT and *Chi*/+ comparisons were performed applying unpaired parametric or non-parametric *t* test. Mineralization was evaluated by three independent blinded operators and defined in specific classes (beginning/no mineralization, incomplete mineralization, complete mineralization). Categorical variables were summarized by percentage. Differences in mineralization between treatments and genotypes were evaluated with Chi-squared test. For statistic significance, P value <0.05 was considered. All the analyses were performed using STATA 12®.

Supplementary Material

Supplementary Material is available at *HMG* online.

Acknowledgements

We thank Dr Patrizia Vaghi, Centro Grandi Strumenti, University of Pavia, Italy, for technical assistance with confocal microscopy and the animal facility 'Centro di servizio per la gestione unificata delle attività di stabulazione e di radiobiologia' of the University of Pavia.

Conflict of Interest statement. None declared.

Funding

The work was supported by Fondazione Cariplo (grant No. 2013-0612), Telethon (grant No. GGP13098) and the European Community, FP7, 'Sybil' project (grant No. 602300). Funding to pay the Open Access publication charges for this article was provided by Fondazione Telethon.

References

1. Forlino, A., Cabral, W.A., Barnes, A.M. and Marini, J.C. (2011) New perspectives on osteogenesis imperfecta. *Nat. Rev. Endocrinol.*, **7**, 540–557.
2. Forlino, A. and Marini, J.C. (2016) Osteogenesis imperfecta. *Lancet*, **387**, 1657–1671.
3. Forlino, A., Tani, C., Rossi, A., Lupi, A., Campari, E., Gualeni, B., Bianchi, L., Armini, A., Cetta, G., Bini, L. *et al.* (2007) Differential expression of both extracellular and intracellular proteins is involved in the lethal or nonlethal phenotypic variation of BrtlIV, a murine model for osteogenesis imperfecta. *Proteomics*, **7**, 1877–1891.
4. Mertz, E.L., Makareeva, E., Mirigian, L.S., Koon, K.Y., Perosky, J.E., Kozloff, K.M. and Leikin, S. (2016) Makings of a brittle bone: unexpected lessons from a low protein diet study of a mouse OI model. *Matrix. Biol.*, **52–54**, 29–42.
5. Bianchi, L., Gagliardi, A., Gioia, R., Besio, R., Tani, C., Landi, C., Cipriano, M., Gimigliano, A., Rossi, A., Marini, J.C. *et al.*

(2012) Differential response to intracellular stress in the skin from osteogenesis imperfecta Brtl mice with lethal and non lethal phenotype: a proteomic approach. *J. Proteomics*, **75**, 4717–4733.
6. Forlino, A., Porter, F.D., Lee, E.J., Westphal, H. and Marini, J.C. (1999) Use of the Cre/lox recombination system to develop a non-lethal knock-in murine model for osteogenesis imperfecta with an alpha1(I) G349C substitution. Variability in phenotype in BrtlIV mice. *J. Biol. Chem.*, **274**, 37923–37931.
7. Bianchi, L., Gagliardi, A., Maruelli, S., Besio, R., Landi, C., Gioia, R., Kozloff, K.M., Khoury, B.M., Coucke, P.J., Symoens, S. *et al.* (2015) Altered cytoskeletal organization characterized lethal but not surviving Brtl+/- mice: insight on phenotypic variability in osteogenesis imperfecta. *Hum. Mol. Genet.*, **24**, 6118–6133.
8. Daley, E., Streeten, E.A., Sorkin, J.D., Kuznetsova, N., Shapses, S.A., Carleton, S.M., Shuldiner, A.R., Marini, J.C., Phillips, C.L., Goldstein, S.A. *et al.* (2010) Variable bone fragility associated with an Amish COL1A2 variant and a knock-in mouse model. *J. Bone Miner. Res.*, **25**, 247–261.
9. Mirigian, L.S., Makareeva, E., Mertz, E.L., Omari, S., Roberts-Pilgrim, A.M., Oestreich, A.K., Phillips, C.L. and Leikin, S. (2016) Osteoblast malfunction caused by cell stress response to procollagen misfolding in alpha2(I)-G610C mouse model of osteogenesis imperfecta. *J. Bone Miner. Res.*, **31**, 1608–1616.
10. Nosengo, N. (2016) Can you teach old drugs new tricks? *Nature*, **534**, 314–316.
11. Matoori, S. and Leroux, J.C. (2015) Recent advances in the treatment of hyperammonemia. *Adv. Drug. Deliv. Rev.*, **90**, 55–68.
12. Wagner, M. and Trauner, M. (2016) Recent advances in understanding and managing cholestasis. [version 1; referees 2 approved] *F1000Res*, **5**, 705.
13. Iannitti, T. and Palmieri, B. (2011) Clinical and experimental applications of sodium phenylbutyrate. *Drugs R D*, **11**, 227–249.
14. Fass, D.M., Shah, R., Ghosh, B., Hennig, K., Norton, S., Zhao, W.N., Reis, S.A., Klein, P.S., Mazitschek, R., Maglathlin, R.L. *et al.* (2010) Effect of inhibiting histone deacetylase with short-chain carboxylic acids and their hydroxamic acid analogs on vertebrate development and neuronal chromatin. *ACS Med. Chem. Lett.*, **2**, 39–42.
15. Vang, S., Longley, K., Steer, C.J. and Low, W.C. (2014) The unexpected uses of urso- and tauroursodeoxycholic acid in the treatment of non-liver diseases. *Glob. Adv. Health Med.*, **3**, 58–69.
16. MacRae, C.A. and Peterson, R.T. (2015) Zebrafish as tools for drug discovery. *Nat. Rev. Drug Discov.*, **14**, 721–731.
17. Howe, K., Clark, M.D., Torroja, C.F., Torrance, J., Berthelot, C., Muffato, M., Collins, J.E., Humphray, S., McLaren, K., Matthews, L. *et al.* (2013) The zebrafish reference genome sequence and its relationship to the human genome. *Nature*, **496**, 498–503.
18. Flicek, P., Amode, M.R., Barrell, D., Beal, K., Billis, K., Brent, S., Carvalho-Silva, D., Clapham, P., Coates, G., Fitzgerald, S. *et al.* (2014) Ensembl 2014. *Nucleic Acids Res.*, **42**, D749–D755.
19. Moro, E., Vettori, A., Porazzi, P., Schiavone, M., Rampazzo, E., Casari, A., Ek, O., Facchinello, N., Astone, M., Zancan, I. *et al.* (2013) Generation and application of signaling pathway reporter lines in zebrafish. *Mol. Genet. Genomics*, **288**, 231–242.
20. Blum, M., De Robertis, E.M., Wallingford, J.B. and Niehrs, C. (2015) Morpholinos: antisense and Sensibility. *Dev. Cell*, **35**, 145–149.
21. Gonzales, A.P. and Yeh, J.R. (2014) Cas9-based genome editing in zebrafish. *Methods Enzymol.*, **546**, 377–413.
22. Fisher, S., Jagadeeswaran, P. and Halpern, M.E. (2003) Radiographic analysis of zebrafish skeletal defects. *Dev. Biol.*, **264**, 64–76.
23. Braasch, I., Gehrke, A.R., Smith, J.J., Kawasaki, K., Manousaki, T., Pasquier, J., Amores, A., Desvignes, T., Batzel, P., Catchen, J. *et al.* (2016) The spotted gar genome illuminates vertebrate evolution and facilitates human-teleost comparisons. *Nat. Genet.*, **48**, 427–437.
24. Li, N., Felber, K., Elks, P., Croucher, P. and Roehl, H.H. (2009) Tracking gene expression during zebrafish osteoblast differentiation. *Dev. Dyn.*, **238**, 459–466.
25. Weigele, J. and Franz-Odendaal, T.A. (2016) Functional bone histology of zebrafish reveals two types of endochondral ossification, different types of osteoblast clusters and a new bone type. *J. Anat.*, **229**, 92–103.
26. Garbes, L., Kim, K., Riess, A., Hoyer-Kuhn, H., Beleggia, F., Bevot, A., Kim, M.J., Huh, Y.H., Kweon, H.S., Savarirayan, R. *et al.* (2015) Mutations in SEC24D, encoding a component of the COPII machinery, cause a syndromic form of osteogenesis imperfecta. *Am. J. Hum. Genet.*, **96**, 432–439.
27. Kamoun-Goldrat, A.S. and Le Merrer, M.F. (2007) Animal models of osteogenesis imperfecta and related syndromes. *J. Bone Miner. Metab.*, **25**, 211–218.
28. Gistelinck, C., Eckhard Witten, P., Huysseune, A., Symoens, S., Malfait, F., Larionova, D., Simoens, P., Dierick, M., Van Hoorebeke, L., D., Paepe, A. *et al.* (2016) Loss of type I collagen telopeptide lysyl hydroxylation causes musculoskeletal abnormalities in a Zebrafish model of Bruck syndrome. *J. Bone Miner. Res.*, **31**, 1930.
29. Cho, S.Y., Asharani, P.V., Kim, O.H., Iida, A., Miyake, N., Matsumoto, N., Nishimura, G., Ki, C.S., Hong, G., Kim, S.J. *et al.* (2015) Identification and in vivo functional characterization of novel compound heterozygous BMP1 variants in osteogenesis imperfecta. *Hum. Mutat.*, **36**, 191–195.
30. Fleming, A., Sato, M. and Goldsmith, P. (2005) High-throughput in vivo screening for bone anabolic compounds with zebrafish. *J. Biomol. Screen*, **10**, 823–831.
31. Duran, I., Mari-Beffa, M., Santamaria, J.A., Becerra, J. and Santos-Ruiz, L. (2011) Actinotrichia collagens and their role in fin formation. *Dev. Biol.*, **354**, 160–172.
32. Gistelinck, C., Gioia, R., Gagliardi, A., Tonelli, F., Marchese, L., Bianchi, L., Landi, C., Bini, L., Huysseune, A., Witten, P.E. *et al.* (2016) Zebrafish collagen type I: molecular and biochemical characterization of the major structural protein in bone and skin. *Sci. Rep.*, **6**, 21540.
33. Ito, S. and Nagata, K. (2017) Biology of Hsp47 (Serpin H1), a collagen-specific molecular chaperone. *Semin. Cell. Dev. Biol*, **62**, 142–151.
34. Ishikawa, Y., Ito, S., Nagata, K., Sakai, L.Y. and Bachinger, H.P. (2016) Intracellular mechanisms of molecular recognition and sorting for transport of large extracellular matrix molecules. *Proc. Natl. Acad. Sci. U.S.A.*, **113**, E6036–E6044.
35. Lisse, T.S., Thiele, F., Fuchs, H., Hans, W., Przemeck, G.K., Abe, K., Rathkolb, B., Quintanilla-Martinez, L., Hoelzlwimmer, G., Helfrich, M. *et al.* (2008) ER stress-mediated apoptosis in a new mouse model of osteogenesis imperfecta. *PLoS Genet.*, **4**, e7.
36. Chen, F., Guo, R., Itoh, S., Moreno, L., Rosenthal, E., Zappitelli, T., Zirngibl, R.A., Flenniken, A., Cole, W., Grynpas, M. *et al.* (2014) First mouse model for combined osteogenesis imperfecta and Ehlers-Danlos syndrome. *J. Bone Miner. Res.*, **29**, 1412–1423.
37. Marlowe, A., Pepin, M.G. and Byers, P.H. (2002) Testing for osteogenesis imperfecta in cases of suspected non-accidental injury. *J. Med. Genet.*, **39**, 382–386.

38. Makareeva, E., Mertz, E.L., Kuznetsova, N.V., Sutter, M.B., DeRidder, A.M., Cabral, W.A., Barnes, A.M., McBride, D.J., Marini, J.C. and Leikin, S. (2008) Structural heterogeneity of type I collagen triple helix and its role in osteogenesis imperfecta. *J. Biol. Chem.*, **283**, 4787–4798.
39. Morvan-Dubois, G., Le Guellec, D., Garrone, R., Zylberberg, L. and Bonnaud, L. (2003) Phylogenetic analysis of vertebrate fibrillar collagen locates the position of zebrafish alpha3(I) and suggests an evolutionary link between collagen alpha chains and hox clusters. *J. Mol. Evol.*, **57**, 501–514.
40. Forlino, A., Kuznetsova, N.V., Marini, J.C. and Leikin, S. (2007) Selective retention and degradation of molecules with a single mutant alpha1(I) chain in the Brtl IV mouse model of OI. *Matrix Biol.*, **26**, 604–614.
41. Gioia, R., Panaroni, C., Besio, R., Palladini, G., Merlini, G., Giansanti, V., Scovassi, I.A., Villani, S., Villa, I., Villa, A. *et al.* (2012) Impaired osteoblastogenesis in a murine model of dominant osteogenesis imperfecta: a new target for osteogenesis imperfecta pharmacological therapy. *Stem Cells*, **30**, 1465–1476.
42. Gorman, K.F. and Breden, F. (2007) Teleosts as models for human vertebral stability and deformity. *Comp. Biochem. Physiol. C Toxicol. Pharmacol.*, **145**, 28–38.
43. Fleming, A., Keynes, R. and Tannahill, D. (2004) A central role for the notochord in vertebral patterning. *Development*, **131**, 873–880.
44. Duran, I., Csukasi, F., Taylor, S.P., Krakow, D., Becerra, J., Bombarely, A. and Mari-Beffa, M. (2015) Collagen duplicate genes of bone and cartilage participate during regeneration of zebrafish fin skeleton. *Gene Expr. Patterns*, **19**, 60–69.
45. Wood, A. (1982) Early pectoral fin development and morphogenesis of the apical ectodermal ridge in the killifish, Aphyosemion scheeli. *Anat. Rec.*, **204**, 349–356.
46. Wood, A. and Thorogood, P. (1984) An analysis of in vivo cell migration during teleost fin morphogenesis. *J. Cell. Sci.*, **66**, 205–222.
47. Kozloff, K.M., Carden, A., Bergwitz, C., Forlino, A., Uveges, T.E., Morris, M.D., Marini, J.C. and Goldstein, S.A. (2004) Brittle IV mouse model for osteogenesis imperfecta IV demonstrates postpubertal adaptations to improve whole bone strength. *J. Bone Miner. Res.*, **19**, 614–622.
48. Shapiro, J.R., Byers, P.H., Glorieux, F.H. and Sponseller, P.D. (2013) *Osteogenesis Imperfecta. A Translational Approach to Brittle Bone Disease*. Elsevier, The Netherlands.
49. Besio, R. and Forlino, A. (2015) New frontiers for dominant osteogenesis imperfecta treatment: gene/cellular therapy approaches. *Adv Regenerative Biol.*, **2**, 27964.
50. Rousseau, J., Gioia, R., Layrolle, P., Lieubeau, B., Heymann, D., Rossi, A., Marini, J.C., Trichet, V. and Forlino, A. (2014) Allele-specific Col1a1 silencing reduces mutant collagen in fibroblasts from Brtl mouse, a model for classical osteogenesis imperfecta. *Eur. J. Hum. Genet.*, **22**, 667–674.
51. Lindahl, K., Kindmark, A., Laxman, N., Astrom, E., Rubin, C.J. and Ljunggren, O. (2013) Allele dependent silencing of collagen type I using small interfering RNAs targeting 3'UTR Indels - a novel therapeutic approach in osteogenesis imperfecta. *Int. J. Med. Sci.*, **10**, 1333–1343.
52. Boot-Handford, R.P. and Briggs, M.D. (2010) The unfolded protein response and its relevance to connective tissue diseases. *Cell. Tissue Res.*, **339**, 197–211.
53. Makareeva, E., Aviles, N.A. and Leikin, S. (2011) Chaperoning osteogenesis: new protein-folding disease paradigms. *Trends Cell. Biol.*, **21**, 168–176.
54. Briggs, M.D., Bell, P.A., Wright, M.J. and Pirog, K.A. (2015) New therapeutic targets in rare genetic skeletal diseases. *Expert. Opin. Orphan. Drugs*, **3**, 1137–1154.
55. Gray, R.S., Wilm, T.P., Smith, J., Bagnat, M., Dale, R.M., Topczewski, J., Johnson, S.L. and Solnica-Krezel, L. (2014) Loss of col8a1a function during zebrafish embryogenesis results in congenital vertebral malformations. *Dev. Biol.*, **386**, 72–85.
56. Huang, C.C., Wang, T.C., Lin, B.H., Wang, Y.W., Johnson, S.L. and Yu, J. (2009) Collagen IX is required for the integrity of collagen II fibrils and the regulation of vascular plexus formation in zebrafish caudal fins. *Dev. Biol.*, **332**, 360–370.
57. Shen, B., Mu, J.X. and Pei, F.X. (2007) Relationship among bone mineral density, collagen composition, and biomechanical properties of callus in the healing of osteoporotic fracture. *Chin. J. Traumatol.*, **10**, 360–365.
58. Ishikawa, Y. and Bachinger, H.P. (2013) A molecular ensemble in the rER for procollagen maturation. *Biochim. Biophys. Acta*, **1833**, 2479–2491.
59. Ishida, Y. and Nagata, K. (2009) Autophagy eliminates a specific species of misfolded procollagen and plays a protective role in cell survival against ER stress. *Autophagy*, **5**, 1217–1219.
60. Ishida, Y., Yamamoto, A., Kitamura, A., Lamande, S.R., Yoshimori, T., Bateman, J.F., Kubota, H. and Nagata, K. (2009) Autophagic elimination of misfolded procollagen aggregates in the endoplasmic reticulum as a means of cell protection. *Mol. Biol. Cell*, **20**, 2744–2754.
61. Lee, H.W., Suh, J.H., Kim, A.Y., Lee, Y.S., Park, S.Y. and Kim, J.B. (2006) Histone deacetylase 1-mediated histone modification regulates osteoblast differentiation. *Mol. Endocrinol.*, **20**, 2432–2443.
62. Schroeder, T.M. and Westendorf, J.J. (2005) Histone deacetylase inhibitors promote osteoblast maturation. *J. Bone Miner. Res.*, **20**, 2254–2263.
63. Luo, T., Chen, B. and Wang, X. (2015) 4-PBA prevents pressure overload-induced myocardial hypertrophy and interstitial fibrosis by attenuating endoplasmic reticulum stress. *Chem. Biol. Interact.*, **242**, 99–106.
64. Coulon, S.M., Miller, A.C., Reed, J.M. and Martin, C.K. (2012) Reliability of a common solution-based taste perception test: implications for validity and a briefer test. *Eat Behav.*, **13**, 42–45.
65. Trendowski, M., Wong, V., Wellington, K., Hatfield, S. and Fondy, T.P. (2014) Tolerated doses in zebrafish of cytochalasins and jasplakinolide for comparison with tolerated doses in mice in the evaluation of pre-clinical activity of microfilament-directed agents in tumor model systems in vivo. *In Vivo*, **28**, 1021–1031.
66. de Almeida, S.F., Picarote, G., Fleming, J.V., Carmo-Fonseca, M., Azevedo, J.E. and de Sousa, M. (2007) Chemical chaperones reduce endoplasmic reticulum stress and prevent mutant HFE aggregate formation. *J. Biol. Chem.*, **282**, 27905–27912.
67. Cortez, L. and Sim, V. (2014) The therapeutic potential of chemical chaperones in protein folding diseases. *Prion*, **8**,
68. Parichy, D.M., Elizondo, M.R., Mills, M.G., Gordon, T.N. and Engeszer, R.E. (2009) Normal table of postembryonic zebrafish development: staging by externally visible anatomy of the living fish. *Dev. Dyn.*, **238**, 2975–3015.
69. Walker, M.B. and Kimmel, C.B. (2007) A two-color acid-free cartilage and bone stain for zebrafish larvae. *Biotech. Histochem.*, **82**, 23–28.
70. Lin, Y.Y., White, R.J., Torelli, S., Cirak, S., Muntoni, F. and Stemple, D.L. (2011) Zebrafish Fukutin family proteins link the unfolded protein response with dystroglycanopathies. *Hum. Mol. Genet.*, **20**, 1763–1775.